Polarization-resolved characterization of plasmon waves supported by an anisotropic metasurface

Samusev, Anton; Mukhin, Ivan; Malureanu, Radu; Takayama, Osamu; Permyakov, Dmitry V. ; Sinev, Ivan S.; Baranov, Dmitry ; Yermakov, Oleh; Iorsh, Ivan V.; Bogdanov, Andrey A.; Lavrinenko, Andrei

Published in:
Optics Express

Link to article, DOI:
10.1364/OE.25.032631

Publication date:
2017

Document Version
Publisher's PDF, also known as Version of record

Research Article | Vol. 25, No. 26 | 25 Dec 2017 | OPTICS EXPRESS 32631
Optics EXPRESS

Polarization-resolved characterization of plasmon waves supported by an anisotropic metasurface

ANTON SAMUSEV,[1,*] IVAN MUKHIN,[1,2] RADU MALUREANU,[3,4] OSAMU TAKAYAMA,[3] DMITRY V. PERMYAKOV,[1] IVAN S. SINEV,[1] DMITRY BARANOV,[1] OLEH YERMAKOV,[1] IVAN V. IORSH,[1] ANDREY A. BOGDANOV,[1] AND ANDREI V. LAVRINENKO[1,3]

[1] *Department of Nanophotonics and Metamaterials, ITMO University, St. Petersburg 197101, Russia*
[2] *St. Petersburg Academic University, St. Petersburg 194021, Russia*
[3] *Department of Photonics Engineering, Technical University of Denmark, DK-2800 Kongens Lyngby, Denmark*
[4] *National Centre for Micro- and Nano-Fabrication, Technical University of Denmark, DK-2800 Kongens Lyngby, Denmark*
[*] *a.samusev@metalab.ifmo.ru*

Abstract: Optical metasurfaces have great potential to form a platform for manipulation of surface waves. A plethora of advanced surface-wave phenomena such as negative refraction, self-collimation and channeling of 2D waves can be realized through on-demand engineering of dispersion properties of a periodic metasurface. In this letter, we report on polarization-resolved measurement of dispersion of plasmon waves supported by an anisotropic metasurface. We demonstrate that a subdiffractive array of strongly coupled resonant plasmonic nanoparticles supports both TE and TM plasmon modes at optical frequencies. With the assistance of numerical simulations we identify dipole and quadrupole dispersion bands. The shape of isofrequency contours of the modes changes drastically with frequency exhibiting nontrivial transformations of their curvature and topology that is confirmed by the experimental data. By revealing polarization degree of freedom for surface waves, our results open new routes for designing planar on-chip devices for surface photonics.

OCIS codes: (160.3918) Metamaterials; (240.6680) Surface plasmons; (240.6690) Surface waves.

References and links

1. A. Pors, M. G. Nielsen, T. Bernardin, J.-C. Weeber, and S. I. Bozhevolnyi, "Efficient unidirectional polarization-controlled excitation of surface plasmon polaritons," Light Sci. Appl. **3**, e197 (2014).
2. D. Sievenpiper, J. Schaffner, H. Song, R. Loo, and G. Tangonan, "Two-dimensional beam steering using an electrically tunable impedance surface," IEEE Trans. Antennas Propag. **51**, 2713–2722 (2003).
3. H. Lamb, "On the Reflection and Transmission of Electric Waves by a Metallic Grating," Proc. Lond. Math. Soc. **s1-29**, 523–546 (1897).
4. S. B. Glybovski, S. A. Tretyakov, P. A. Belov, Y. S. Kivshar, and C. R. Simovski, "Metasurfaces: From microwaves to visible," Phys. Rep. **634**, 1–72 (2016).
5. M. K. Hedayati, M. Javaherirahim, B. Mozooni, R. Abdelaziz, A. Tavassolizadeh, V. S. K. Chakravadhanula, V. Zaporojtchenko, T. Strunkus, F. Faupel, and M. Elbahri, "Design of a Perfect Black Absorber at Visible Frequencies Using Plasmonic Metamaterials," Adv. Mater. **23**, 5410–5414 (2011).
6. K. Liu, X. Zeng, S. Jiang, D. Ji, H. Song, N. Zhang, and Q. Gan, "A large-scale lithography-free metasurface with spectrally tunable super absorption," Nanoscale **6**, 5599 (2014).
7. Y. Yao, R. Shankar, M. A. Kats, Y. Song, J. Kong, M. Loncar, and F. Capasso, "Electrically Tunable Metasurface Perfect Absorbers for Ultrathin Mid-Infrared Optical Modulators," Nano Lett. **14**, 6526–6532 (2014).
8. G. M. Akselrod, J. Huang, T. B. Hoang, P. T. Bowen, L. Su, D. R. Smith, and M. H. Mikkelsen, "Large-Area Metasurface Perfect Absorbers from Visible to Near-Infrared," Adv. Mater. **27**, 8028–8034 (2015).
9. W. Ding, L. Zhou, and S. Y. Chou, "Enhancement and Electric Charge-Assisted Tuning of Nonlinear Light Generation in Bipolar Plasmonics," Nano Lett. **14**, 2822–2830 (2014).
10. J. Lee, M. Tymchenko, C. Argyropoulos, P.-Y. Chen, F. Lu, F. Demmerle, G. Boehm, M.-C. Amann, A. Alù, and M. A. Belkin, "Giant nonlinear response from plasmonic metasurfaces coupled to intersubband transitions," Nature

#296909 https://doi.org/10.1364/OE.25.032631
Journal © 2017 Received 30 May 2017; revised 3 Nov 2017; accepted 17 Nov 2017; published 14 Dec 2017

Optics EXPRESS

511, 65–69 (2014).
11. A. E. Minovich, A. E. Miroshnichenko, A. Y. Bykov, T. V. Murzina, D. N. Neshev, and Y. S. Kivshar, "Functional and nonlinear optical metasurfaces," Laser Photonics Rev. **9**, 195–213 (2015).
12. N. Yu and F. Capasso, "Flat optics with designer metasurfaces," Nat. Mater. **13**, 139–150 (2014).
13. A. V. Kildishev, A. Boltasseva, and V. M. Shalaev, "Planar Photonics with Metasurfaces," Science **339**, 1289 (2013).
14. J. S. Gomez-Diaz and A. Alù, "Flatland Optics with Hyperbolic Metasurfaces," ACS Photonics **3**, 2211–2224 (2016).
15. M. Khorasaninejad, W. T. Chen, R. C. Devlin, J. Oh, A. Y. Zhu, and F. Capasso, "Metalenses at visible wavelengths: Diffraction-limited focusing and subwavelength resolution imaging," Science **352**, 1190–1194 (2016).
16. G. Chen, K. Zhang, A. Yu, X. Wang, Z. Zhang, Y. Li, Z. Wen, C. Li, L. Dai, S. Jiang, and F. Lin, "Far-field sub-diffraction focusing lens based on binary amplitude-phase mask for linearly polarized light," Opt. Express **24**, 11002 (2016).
17. T. Roy, E. T. F. Rogers, and N. I. Zheludev, "Sub-wavelength focusing meta-lens," Opt. Express **21**, 7577 (2013).
18. F. Qin, K. Huang, J. Wu, J. Teng, C.-W. Qiu, and M. Hong, "A Supercritical Lens Optical Label-Free Microscopy: Sub-Diffraction Resolution and Ultra-Long Working Distance," Adv. Mater. **29**, 1602721 (2016).
19. G. Yuan, E. T. F. Rogers, T. Roy, G. Adamo, Z. Shen, and N. I. Zheludev, "Planar super-oscillatory lens for sub-diffraction optical needles at violet wavelengths," Sci. Rep. **4**, 6333 (2014).
20. T. Taubner, D. Korobkin, Y. Urzhumov, G. Shvets, and R. Hillenbrand, "Near-Field Microscopy Through a SiC Superlens," Science **313**, 1595 (2006).
21. N. Fang, "Sub-Diffraction-Limited Optical Imaging with a Silver Superlens," Science **308**, 534–537 (2005).
22. L. Verslegers, P. B. Catrysse, Z. Yu, J. S. White, E. S. Barnard, M. L. Brongersma, and S. Fan, "Planar Lenses Based on Nanoscale Slit Arrays in a Metallic Film," Nano Lett. **9**, 235–238 (2009).
23. A. Grbic, L. Jiang, and R. Merlin, "Near-Field Plates: Subdiffraction Focusing with Patterned Surfaces," Science **320**, 511–513 (2008).
24. G. Zheng, H. Mühlenbernd, M. Kenney, G. Li, T. Zentgraf, and S. Zhang, "Metasurface holograms reaching 80% efficiency," Nat. Nanotechnol. **10**, 308–312 (2015).
25. W. T. Chen, K. Y. Yang, C. M. Wang, Y. W. Huang, G. Sun, I. D. Chiang, C. Y. Liao, W. L. Hsu, H. T. Lin, S. Sun, L. Zhou, A. Q. Liu, and D. P. Tsai, "High-efficiency broadband meta-hologram with polarization-controlled dual images," Nano Lett. **14**, 225–230 (2014).
26. D. Wen, F. Yue, G. Li, G. Zheng, K. Chan, S. Chen, M. Chen, K. F. Li, P. W. H. Wong, K. W. Cheah, E. Yue Bun Pun, S. Zhang, and X. Chen, "Helicity multiplexed broadband metasurface holograms," Nat. Commun. **6**, 8241 (2015).
27. L. Huang, X. Chen, B. Bai, Q. Tan, G. Jin, T. Zentgraf, and S. Zhang, "Helicity dependent directional surface plasmon polariton excitation using a metasurface with interfacial phase discontinuity," Light Sci. Appl. **2**, e70 (2013).
28. X. Ni, A. V. Kildishev, and V. M. Shalaev, "Metasurface holograms for visible light," Nat. Commun. **4**, 2807 (2013).
29. Y. W. Huang, W. T. Chen, W. Y. Tsai, P. C. Wu, C. M. Wang, G. Sun, and D. P. Tsai, "Aluminum plasmonic multicolor meta-Hologram," Nano Lett. **15**, 3122–3127 (2015).
30. F. Aieta, P. Genevet, M. A. Kats, N. Yu, R. Blanchard, Z. Gaburro, and F. Capasso, "Aberration-Free Ultrathin Flat Lenses and Axicons at Telecom Wavelengths Based on Plasmonic Metasurfaces," Nano Lett. **12**, 4932–4936 (2012).
31. M. Khorasaninejad, W. T. Chen, A. Y. Zhu, J. Oh, R. C. Devlin, D. Rousso, and F. Capasso, "Multispectral chiral imaging with a metalens," Nano Lett. **16**, 4595–4600 (2016).
32. E. Arbabi, A. Arbabi, S. M. Kamali, Y. Horie, and A. Faraon, "Multiwavelength polarization-insensitive lenses based on dielectric metasurfaces with meta-molecules," Optica **3**, 628 (2016).
33. X. Chen, L. Huang, H. Mühlenbernd, G. Li, B. Bai, Q. Tan, G. Jin, C.-W. Qiu, S. Zhang, and T. Zentgraf, "Dual-polarity plasmonic metalens for visible light," Nat. Commun. **3**, 1198 (2012).
34. M. Khorasaninejad, W. T. Chen, A. Y. Zhu, J. Oh, R. C. Devlin, C. Roques-Carmes, I. Mishra, and F. Capasso, "Visible Wavelength Planar Metalenses based on Titanium Dioxide," IEEE J. Sel. Top. Quantum Electron. **23**, 1–16 (2016).
35. H. Zhang, M. Kang, X. Zhang, W. Guo, C. Lv, Y. Li, W. Zhang, and J. Han, "Coherent Control of Optical Spin-to-Orbital Angular Momentum Conversion in Metasurface," Adv. Mater. **29**, 1604252 (2016).
36. Y. U. Lee, I. Ozerov, F. Bedu, J. S. Kim, F. Fages, and J. W. Wu, "Spin- and orbital-Hall effect in cyclic group symmetric metasurface," arXiv preprint arXiv:1607.04806 (2016).
37. G. Li, M. Kang, S. Chen, S. Zhang, E. Y.-B. Pun, K. W. Cheah, and J. Li, "Spin-Enabled Plasmonic Metasurfaces for Manipulating Orbital Angular Momentum of Light," Nano Lett. **13**, 4148–4151 (2013).
38. Y. Liu, Y. Ke, H. Luo, and S. Wen, "Photonic spin Hall effect in metasurfaces: a brief review," Nanophotonics **6**, 51–70 (2016).
39. K. Y. Bliokh, F. J. Rodríguez-Fortuño, F. Nori, and A. V. Zayats, "Spin-orbit interactions of light," Nat. Photonics **9**, 796–808 (2015).
40. F. Cardano and L. Marrucci, "Spin-orbit photonics," Nat. Photonics **9**, 776–778 (2015).
41. R. C. Devlin, A. Ambrosio, D. Wintz, S. L. Oscurato, A. Y. Zhu, M. Khorasaninejad, J. Oh, P. Maddalena, and F. Capasso, "Spin-to-orbital angular momentum conversion in dielectric metasurfaces," Opt. Express **25**, 377 (2017).
42. W. Shu, Y. Ke, Y. Liu, X. Ling, H. Luo, and X. Yin, "Radial spin hall effect of light," Phys. Rev. A **93**, 013839 (2016).
43. O. Y. Yermakov, A. I. Ovcharenko, A. A. Bogdanov, I. V. Iorsh, K. Y. Bliokh, and Y. S. Kivshar, "Spin control of light with hyperbolic metasurfaces," Phys. Rev. B **94**, 075446 (2016).
44. R. W. Wood, "On a remarkable case of uneven distribution of light in a diffraction grating spectrum," Proc. R. Soc.

Optics EXPRESS

London **18**, 269–275 (1902).
45. S. Kitson, W. L. Barnes, and J. Sambles, "Full photonic band gap for surface modes in the visible," Phys. Rev. Lett. **77**, 2670 (1996).
46. M. I. D'yakonov, "New type of electromagnetic wave propagating at an interface," JETP **67**, 714–716 (1988).
47. O. Takayama, L. Crasovan, D. Artigas, and L. Torner, "Observation of Dyakonov Surface Waves," Phys. Rev. Lett. **102**, 043903 (2009).
48. O. Takayama, D. Artigas, and L. Torner, "Lossless directional guiding of light in dielectric nanosheets using Dyakonov surface waves," Nat. Nanotechnol. **9**, 419–424 (2014).
49. M. A. Noginov, "Nano-optics: Steering Dyakonov-like waves," Nat. Nanotechnol. **9**, 414–415 (2014).
50. O. Takayama, E. Shkondin, A. Bodganov, M. E. Aryaee Panah, K. Golenitskii, P. Dmitriev, T. Repän, R. Malureanu, P. Belov, F. Jensen, and A. V. Lavrinenko, "Midinfrared surface waves on a high aspect ratio nanotrench platform," ACS Photonics, arXiv:1704.06108 (2017).
51. Y. Liu and X. Zhang, "Metasurfaces for manipulating surface plasmons," Appl. Phys. Lett. **103**, 141101 (2013).
52. A. A. High, R. C. Devlin, A. Dibos, M. Polking, D. S. Wild, J. Perczel, N. P. de Leon, M. D. Lukin, and H. Park, "Visible-frequency hyperbolic metasurface," Nature **522**, 192–196 (2015).
53. O. Y. Yermakov, A. I. Ovcharenko, M. Song, A. A. Bogdanov, I. V. Iorsh, and Y. S. Kivshar, "Hybrid waves localized at hyperbolic metasurfaces," Phys. Rev. B **91**, 235423 (2015).
54. J. S. Gomez-Diaz, M. Tymchenko, and A. Alù, "Hyperbolic Plasmons and Topological Transitions Over Uniaxial Metasurfaces," Phys. Rev. Lett. **114**, 233901 (2015).
55. D. Correas-Serrano, J. S. Gomez-Diaz, A. A. Melcon, and A. Alù, "Black phosphorus plasmonics: anisotropic elliptical propagation and nonlocality-induced canalization," J. Opt. **18**, 104006 (2016).
56. ZEON Corporation, Electronics Materials Division, ZEP520A, Technical Report, Ver.2 Oct.2010 (2012).
57. D. T. F. Marple, "Refractive Index of ZnSe, ZnTe, and CdTe," J. Appl. Phys. **35**, 539–542 (1964).
58. K. M. McPeak, S. V. Jayanti, S. J. P. Kress, S. Meyer, S. Iotti, A. Rossinelli, and D. J. Norris, "Plasmonic Films Can Easily Be Better: Rules and Recipes," ACS Photonics **2**, 326–333 (2015).
59. I. H. Malitson, "Interspecimen Comparison of the Refractive Index of Fused Silica," J. Opt. Soc. Am. **55**, 1205–1209 (1965).
60. R. Sainidou and F. G. de Abajo, "Plasmon guided modes in nanoparticle metamaterials," Opt. Express **16**, 4499–4506 (2008).
61. Z. Sun, X. Zuo, T. Guan, and W. Chen, "Artificial TE-mode surface waves at metal surfaces mimicking surface plasmons," Opt. Express **22**, 4714–4722 (2014).
62. D. Sievenpiper, L. Zhang, R. F. J. Broas, N. G. Alexopolous, and E. Yablonovitch, "High-impedance electromagnetic surfaces with a forbidden frequency band," IEEE Trans. Microwave Theory Tech. **47**, 2059–2074 (1999).
63. A. Poddubny, I. Iorsh, P. Belov, and Y. Kivshar, "Hyperbolic metamaterials," Nat. Photonics **7**, 948–957 (2013).
64. Y. Yang, L. Jing, L. Shen, Z. Wang, B. Zheng, H. Wang, E. Li, N.-H. Shen, T. Koschny, C. M. Soukoulis, and H. Chen, "Hyperbolic spoof plasmonic metasurfaces," NPG Asia Mater. **9**, e428 (2017).
65. A. B. Evlyukhin, T. Fischer, C. Reinhardt, and B. N. Chichkov, "Optical theorem and multipole scattering of light by arbitrarily shaped nanoparticles," Phys. Rev. B **94**, 205434 (2016).

1. Introduction

Metasurfaces are a two-dimensional analogue of bulk metamaterials. They represent a dense array (usually periodic) of subwavelength scatterers, [1] which are often called meta-atoms. The term *metasurface* was introduced recently [2], but such objects are fairly well-known in electromagnetism as *impedance* or *frequency selective surfaces*. They have been actively studied for more than 100 years [3] aiming radio frequencies and microwaves.

Nowadays, metasurfaces are intensively studied in optics and photonics, because they possess many properties of bulk metamaterials being, at the same time, much less lossy, cheaper to fabricate, fully compatible with planar technologies, and ready to be implanted in modern on-chip devices. They offer unprecedented control over phase, amplitude, polarization, propagation directions, and wavefront features of reflected and transmitted waves [4]. In particular, metasurfaces could essentially increase harvesting of solar energy [5–8] and enhance nonlinear response in optics [9–11]. The actively developed physics of metasurfaces results in formation of such branches of optics as *flat optics* and *planar photonics* [12–14]. The concept of phase discontinuities, the generalized Snell's and Brewster's laws make metasurfaces very promising for a plethora of applications such as subwavelength focusing and imaging [15–21], flat lenses [12, 22, 23] and holograms [24–29], aberration-free, multispectral chiral metalenses, helicity-dependent, and polarization-insensitive lenses [30–34], light modulators providing efficient control over orbital

Optics EXPRESS

and spin angular momentum of light [35–43].

The majority of the results reported so far are related to free space optics with functioning of metasurfaces in the transverse configuration. In this case the leaky and quasi-guided resonances play a major role [44, 45]. However, for on-chip photonic applications, metasurfaces are expected to operate in the in-plane mode, when the surface modes move to the forefront. For routing of optical signals and all-optical networking, the precise control over directivity of surface waves is needed. One of the ways is to involve Dyakonov surfaces waves, since high directivity is their intrinsic feature [46–50]. However, their weak localization and very specific existence conditions impede large-scale implementation of Dyakonov waves in photonic circuits.

Alternatively, it is possible to exploit the conventional SPPs whose directivity and wave fronts can be engineered via nanostructuring of plasmonic interfaces. In [51] Liu and Zhang showed that isofrequency contours of SPPs propagating along a metallic grating can have elliptic, flat, or hyperbolic shape depending on geometry of the grating. This results in broadband negative refraction and non-divergent propagation of SPPs. A visible-frequency non-resonant hyperbolic metasurface based on a nanometer-scale silver/air grating was implemented in [52].

Recently, it has been predicted that the spectrum of a resonant metasurface described in terms of local anisotropic surface conductivity tensor consists of two hybrid TE-TM polarized modes that can be classified as TE-like and TM-like plasmons [53, 54]. Their isofrequency contours are of elliptic, hyperbolic, 8-shaped, rhombic, or arc form depending on the frequency. Such variety of shapes can support diverse phenomena, e.g. negative refraction, self-collimation, channeling of surface waves, and a giant enhancement of spontaneous emission of quantum emitters due to the large density of optical states. The similar phenomena can be observed for metasurfaces implemented using nanostructured graphene monolayers and naturally anisotropic ultrathin black phosphorus films [14, 54, 55].

In this work, we report the characterization of a resonant anisotropic plasmonic metasurface consisting of a dense array of thin gold elliptic nanodisks supporting propagation of plasmon modes in the optical range. We characterize dispersion of both TE- and TM-like plasmons with attenuated total internal reflection spectroscopy and reveal topological transition of their isofrequency contours.

2. Fabrication and characterization

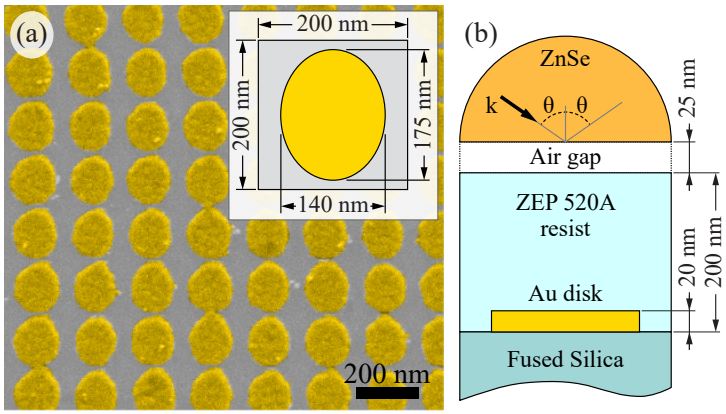

Fig. 1. (a) False color scanning electron micrograph of a small region of the metasurface sample (image taken before sputtering of the cover layer). The inset shows the unit cell used in numerical simulations. (b) Schematic of the experimental geometry for surface waves spectroscopy in Otto configuration.

Optics EXPRESS

The anisotropic metasurface was fabricated on a fused silica substrate using electron beam lithography followed by thermal evaporation of a 20 nm thick layer of gold and a lift-off process. The fabricated structure is a 200×200 μm^2 array of cylindrical gold nanodisks with the elliptical base. The period of the array is 200 nm in both directions, while the long and short axes of the nanodisks are 175 and 140 nm, respectively [see Fig. 1(a)]. To facilitate surface waves propagation in the symmetric environment, the sample was subsequently covered by a 200 nm layer of transparent resist (ZEP 520A) with the refractive index closely matching that of silicon oxide in the visible and near-IR spectral regions [56].

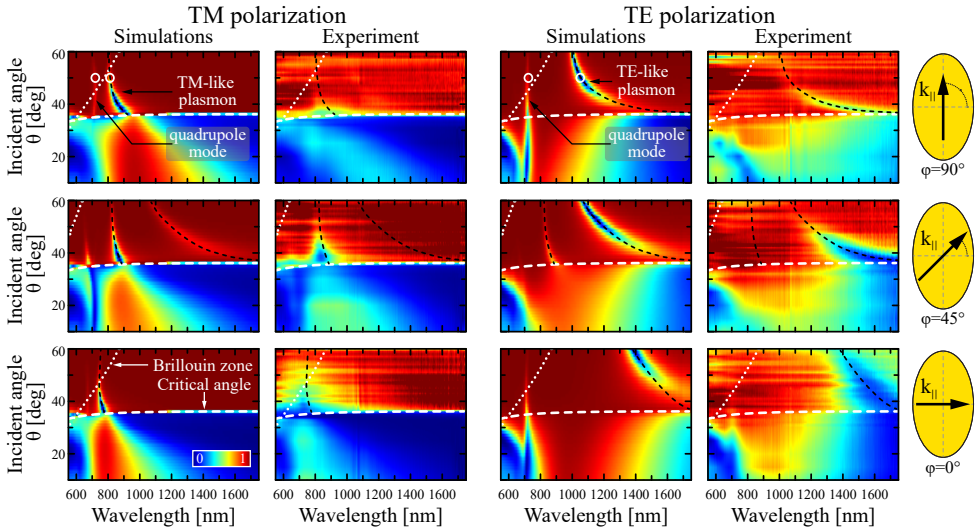

Fig. 2. Measured and simulated angular dependencies of the reflectance spectra of the anisotropic metasurface coupled to a high-index ZnSe prism. The data are presented for both TM- and TE-polarized excitation (left and right column couples, respectively). Top, middle and bottom rows correspond to the plane of incidence forming an azimuthal angle φ of 90°, 45°, and 0° with the short axis of elliptic particles, as sketched at the right. The wavelength-dependent critical angle for the ZnSe-resist interface is shown with the white dashed line. The white dotted line stands for the edge of the first Brillouin zone. The black dashed curves indicating surface waves are given for eye guiding. Different types of surface modes are designated with circles.

To characterize the dispersion of the surface waves we resorted to attenuated total internal reflection spectroscopy in Otto geometry [see Fig. 1(b)]. To excite the surface waves, one needs to provide the wavevectors of the exciting wave residing under the light line of the dielectric environment of the metasurface (*i.e.*, silicon oxide substrate and resist superlayer). For this purpose, we used a zinc selenide (ZnSe) hemicylindrical prism with the refractive index of around 2.48 in the near-IR range [57]. The sample was attached to the prism with a polymer screw to minimize the weakly controllable air gap between the sample and ZnSe interfaces [see the inset in Fig. 1(b)]. In this configuration (known as the Otto geometry), surface waves can be excited via evanescent coupling of light incident at the ZnSe-sample interface at angles greater than the critical angle, which is about 36° in the spectral range of interest. By measuring reflectance spectra at different angles of incidence θ, it is possible to reconstruct dispersion of surface waves excited at the metasurface.

In the experiment, the sample was illuminated by a supercontinuum laser source (NKT Photonics SuperK Extreme) polarized with a Glan-Taylor prism and focused by a series of

Optics EXPRESS

parabolic mirrors on the sample surface through a ZnSe prism to a spot of approximately 150 μm in size. The reflected light was collected with another parabolic mirror and then sent to a spectrometer (Ando AQ-6315E) through an optical fiber. The sample and the collection optics were mounted on separate rotation stages, which allowed for reflectance spectra measurements in a broad range of incident angles (from 10° up to 60°).

Numerical simulations mimicking the experiment were carried out using the frequency-domain solver of the COMSOL Multiphysics package. The simulation cell with periodic boundary conditions in both directions is shown schematically in Fig. 1(b). The exact dimensions of the structure were verified by means of scanning electron microscopy [Fig. 1(a)]. The refractive indices of the materials were obtained from literature (ZEP 520A [56], zinc selenide [57], gold [58], and fused silica [59]). The size of the air gap in the simulations was chosen to be 25 nm accordingly to the best matching of the simulated spectra with the experimental ones.

3. Discussion

Figure 2 shows the experimental and simulated reflectance maps plotted in "wavelength - angle of incidence" axes for both the TE- and TM-polarized excitations and three azimuthal angles $\varphi = 0°, 45°, 90°$ describing orientation of the plane of incidence with respect to the long axis of the nanodisks. The measured reflectance maps demonstrate good correspondence with the simulated ones for all considered cases. Some discrepancy can be attributed to inhomogeneities of the sample and the deviations of the air gap size in the experiment.

The reflectance maps demonstrate a rich variety of near- and far-field features corresponding to the regions above and below the critical angle, respectively. The pronounced reflectance dips above the critical angle stand for the surface modes supported by the metasurface. In the near-IR range ($\lambda > 750$ nm), two types of surface waves are excited: a short-wavelength TM-like plasmon and a long-wavelength TE-like plasmon [60, 61]. Observation of these two types of plasmons agrees with the predictions of the local analytical model for resonant anisotropic metasurface [53]. The spectral position of the reflectance dips corresponding to these modes strongly depends on the orientation of the sample, clearly demonstrating the anisotropy of their dispersion. The TE-like mode has no frequency cut-off and can propagate at arbitrary low frequencies, where its dispersion curve asymptotically tends to the light line. This means that the mode becomes weakly confined and leaks into the ZnSe prism. It results in broadening of the resonance and decrease of its intensity. The TM-like mode residing in the shorter wavelength region has a cutoff frequency that depends on the propagation direction. Importantly, due to controllable dispersion both TE- and TM-like plasmons can exhibit wavevectors and density of optical states larger than that of plasmons at gold-air interface. These properties are essential for high-resolution imaging and sensing.

The origin of the two-dimensional TE- and TM-like plasmons is the following. The TE-like mode is formed due to the coupling of electric dipoles induced in the plasmonic nanodisks in the direction perpendicular to the wavevector of surface wave. Existence of such mode is possible only for the negative polarizability of the plasmonic particles [62], i.e. at the frequencies lower than their plasmon resonance [53]. The TM-like mode is formed due to the coupling of the dipoles oriented along the propagation direction. Existence of such mode is possible only for the positive polarizability of the plasmonic particles, i.e. at the frequencies higher than plasmon resonance [62]. Due to the elliptic shape of the nanodisks and their interaction with neighbors, the degeneracy of the localized plasmon resonance is lifted. This results in pronounced anisotropy of the dispersion of surface modes and in hybridization of their polarization. The latter is seen from the numerical results presented in Fig. 2 (middle row, $\varphi = 45°$). In this direction with low crystallographic symmetry, both TE and TM modes are coupled by incident both TE- and TM-polarized light. This minute effect is not resolved in the measured reflectance maps, which can be attributed to non-optimal prism-to-sample distance realized in the experiment.

Optics EXPRESS

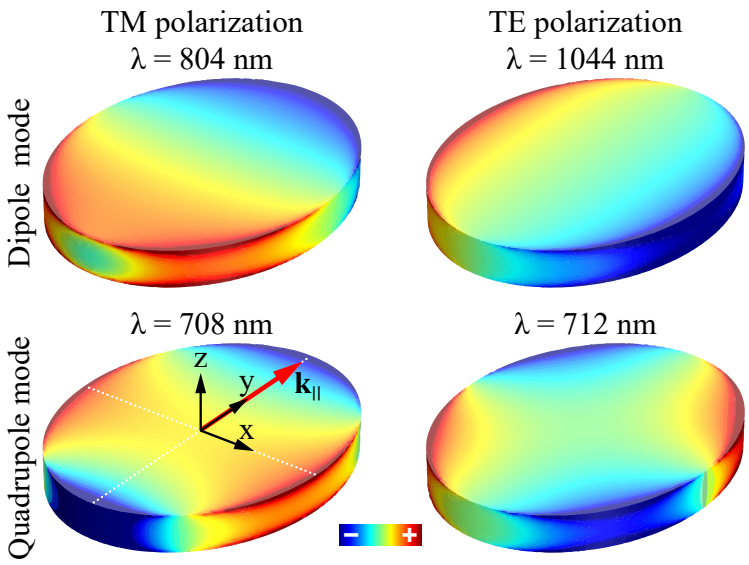

Fig. 3. Simulated surface charge density distributions corresponding to the dipole (a, b) and quadrupole (c, d) surface modes excited in the metasurface by TM- (a, c) and TE-polarized (b, d) incident light. The plane of incidence is parallel to the long axis of elliptical particles. The incident wavevector forms an angle of $\theta = 50^\circ$ with surface normal. The respective reflectance dips associated with surface modes excitation are marked with circles in Fig. 2.

The dipole plasmon resonances are clearly manifested at small angles of incidence (below the critical angle) in both polarizations as the broad peaks. Strong dependence of their spectral position on orientation of the metasurface and polarization of the excitation wave confirms non-degeneracy of the dipole plasmon resonances of the nanodisks.

The surface modes of plasmonic metasurfaces can be also formed due to the coupling of higher multipole plasmon resonances, e.g., quadrupolar, octupolar etc [1]. The reflectance maps shown in Fig. 2 contain additional quadrupole branches near 700 nm, observed under both TM- and TE-polarized excitation. These modes are characterized by barely visible dispersion (low group velocity) and a narrow spectral half-width both above and below the critical angle. The in-plane quadrupole modes in a thin nanodisk are dark modes for the normal excitation.

The calculated surface charge density for TE- and TM-like plasmons plotted in Figs. 3(a), 3(b) verify that the modes are formed due to coupling of the dipole plasmon resonances of the nanodisks, which is also confirmed by multipole decomposition (Table 1). The quadrupole nature of the modes near 700 nm becomes apparent from both surface charge density profiles [Figs. 3(c), 3(d)] and multipole decomposition (Table 1). Almost dispersionless behavior of the quadrupole modes is due to stronger field localization and weaker interaction between neighboring particles in comparison with the dipole modes.

Anisotropic properties of the plasmon modes are manifested most clearly in isofrequency contours plotted within the first Brillouin zone. Figure 4 demonstrates spectral evolution of the isofrequency contours calculated numerically for both TM- and TE-like surface waves. These contours are exhibited as the blue curves lying between the light circles of glass-resist and ZnSe. To compare the calculated isofrequency contours with the experimental data, we extract the position (ω, k) of the reflectance minima corresponding to the surface waves from the measured reflectance maps for three orientations of the sample. The extracted points are shown with crosses imposed on the isofrequency contours in Fig. 4 and demonstrate decent agreement with numerically calculated reflectance minima. The discrepancies observed in the short-wavelength

Optics EXPRESS

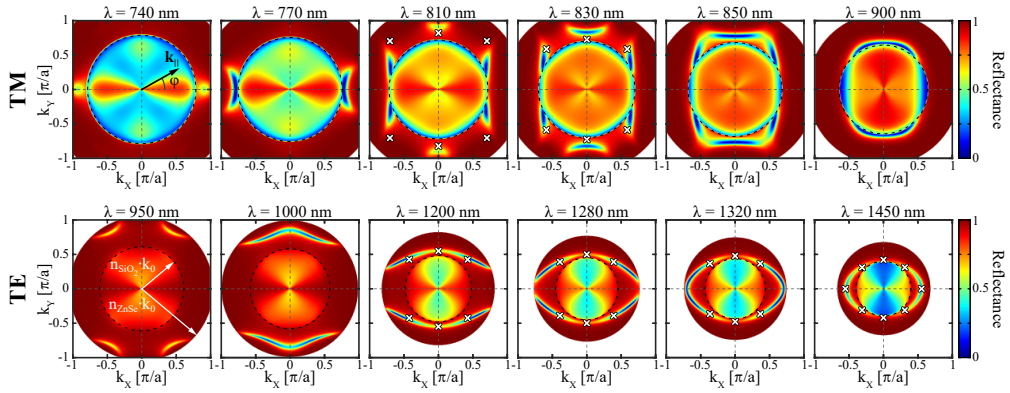

Fig. 4. Reciprocal space reflectance maps for TM- (top row) and TE-polarized (bottom row) light demonstrating spectral evolution of isofrequency contours of surface waves. The maps are plotted within first Brillouin zone. The largest absolute value of available wavevectors (outer circular edge of the definition area) corresponds to the light circle in ZnSe. The inner dashed black circle indicates light wavevector in fused silica substrate. The surface states reside between these circles. Crosses denote the experimental data.

region are most likely to be concerned with the inaccuracy of the model of gold permittivity dispersion.

At low frequencies, far from the plasmon resonance, the anisotropy is vanishingly small, and an isofrequency contour of the TE-like plasmon is very close to a circle. With the increase of the frequency the circle clearly transforms into the ellipse ($\lambda = 1450$ nm). Then the contour ruptures giving rise to a forbidden range of propagation directions along the x-axis ($\lambda = 1280$ nm). At higher frequencies ($\lambda = 950$ nm) TE-like plasmon can propagate only in narrow angular bands in the vicinity of the diagonals of the Brillouin zone. Directivity of the TM-like plasmon (allowed angular band) demonstrates even more dramatic evolution with the change of the wavelength. Near the frequency cutoff ($\lambda \approx 900$ nm) the surface wave propagates nearly along the long axis of the nanodisks completely vanishing in the other directions. At higher frequencies ($\lambda \approx 750$ nm) it propagates only along the short axis of the nanodisks. Such a tunability can be exploited for on-chip routing of optical signals.

The form of the isofrequency contours predicts the relationship between the group and phase velocities and defines the shape of the wavefront and character of propagation [63, 64]. For example, a positive curvature corresponds to the divergent propagation, a negative curvature corresponds to the self-collimated propagation, a flat contour corresponds to the non-diffractive regime. So, the TM-like plasmon demonstrates self-focusing along the long axis of the nanodisks at $\lambda = 830$ nm and along the short axis at $\lambda = 770$ nm, when the hyperbolic regime takes place. Therefore, the considered metasurface support elliptic, hyperbolic, and more complex dispersion regimes, which could be fine-tailored at the fabrication stage by deliberate shaping of the particles.

4. Summary

To conclude, we have studied dispersion and polarization properties of the surface waves supported by a thin metasurface composed of resonant plasmonic nanoparticles. The particles are arranged in a dense square array with a subwavelength period. They have the shape of elliptic cylinders, and due to such shape the metasurface exhibits strong anisotropic properties. The metasurface has been characterized by means of polarization-resolved total internal reflection spectroscopy in the broad range of wavelengths between 600 nm and 1600 nm under different angles of incidence and

Optics EXPRESS

orientations of the structure. Existence of the resonant surface waves with anisotropic dispersion bands has been confirmed. The striking difference with the case of metal-dielectric interfaces is that along with the expected TM-like plasmons the structure supports the TE-like surface states, both maintaining the highly directional propagation regime. Full-vectorial simulations consistently support our findings.

For both types of waves we have analyzed the spectral evolution of the isofrequency contours. Highly nontrivial and polarization-dependent transformation of the contours has been observed. Numerical analysis helped us to classify the principle bands as tightly bound electric dipole resonances. We have also shown that such metasurface supports quadrupole modes with extremely weak dispersion due to weak interparticle coupling. Our findings on a resonant anisotropic metasurface supporting directional and polarization-dependent surface waves provide a flexible platform for on-chip surface photonics for various applications, such as processing and routing of optical signals in quantum communication systems, high-resolution sensing and enhancement of non-linear processes.

Appendix

Table 1 demonstrates contribution of dipole and quadrupole moments obtained from multipole decomposition of the polarization within the single gold nanoparticle of the metasurface. The plane of incidence is parallel to the long axis of elliptical particles. The angle of incidence is $\theta = 50°$ (see Fig. 2). The components of electric dipole and quadrupole moments of the particle are obtained using the following relations [65]:

$$\mathbf{p} = \int \mathbf{P}(\mathbf{r}) d\mathbf{r},$$

$$\hat{Q} = 3 \int \left[\mathbf{r} \otimes \mathbf{P}(\mathbf{r}) + \mathbf{P}(\mathbf{r}) \otimes \mathbf{r} - \frac{2}{3} \left[\mathbf{r} \cdot \mathbf{P}(\mathbf{r}) \right] \hat{U} \right] d\mathbf{r},$$

where $\hat{U}$ is the 3×3 unit tensor. The distributions of the polarization within the unit cell have been taken from the numerical simulations. The magnitude of electric field of the incident wave is 1 [V/m].

Table 1. Dipole and quadrupole moments of gold nanoparicles corresponding to different surface modes excited at the metasurface.

	TM-polarization	TE-polarization
Dipole Mode	λ = 804 nm $\mathbf{p} = (0.0 \quad 24.0 \quad 0.2) \times 10^{-32}$ [C·m] $\hat{Q} = \begin{pmatrix} 1.4 & 0.0 & 0.0 \\ 0.0 & 3.7 & 0.6 \\ 0.0 & 0.6 & 0.0 \end{pmatrix} \times 10^{-39}$ [C·m^2]	λ = 1044 nm $\mathbf{p} = (69.0 \quad 0.0 \quad 0.0) \times 10^{-32}$ [C·m] $\hat{Q} = \begin{pmatrix} 0.0 & 7.1 & 0.9 \\ 7.1 & 0.0 & 0.0 \\ 0.9 & 0.0 & 0.0 \end{pmatrix} \times 10^{-39}$ [C·m^2]
Quadrupole Mode	λ = 708 nm $\mathbf{p} = (0.0 \quad 1.7 \quad 0.2) \times 10^{-32}$ [C·m] $\hat{Q} = \begin{pmatrix} 6.0 & 0.0 & 0.0 \\ 0.0 & 12.8 & 0.2 \\ 0.0 & 0.2 & 0.0 \end{pmatrix} \times 10^{-39}$ [C·m^2]	λ = 712 nm $\mathbf{p} = (1.4 \quad 0.0 \quad 0.0) \times 10^{-32}$ [C·m] $\hat{Q} = \begin{pmatrix} 0.0 & 17.4 & 0.0 \\ 17.4 & 0.0 & 0.0 \\ 0.0 & 0.0 & 0.0 \end{pmatrix} \times 10^{-39}$ [C·m^2]

Funding

O.T., R.M. and A.V.L. acknowledge partial support from the Villum Fonden through "DarkSILD" project No. 11116. The reflectivity measurements and the theoretical part of this work were financially supported by the Russian Science Foundation (No. 15-12-20028).